3202

INSTITUT NATIONAL DE RECHERCHE ET DE SECURITE
Centre de Recherche
Département "Environnement Physique"
Service "Thermique, Ventilation, Eclairage"
Avenue de Bourgogne
B.P. 27
54501 Vandoeuvre Cédex FRANCE

Projet de Publication n° 1342 Avril 1987

DYNAMICAL AND CONTAMINANT FLOW SIMULATION INSIDE VENTILATED INDUSTRIAL PREMISES 1 : NUMERICAL METHODS

J.R. FONTAINE
E. DELLAGI

- Diffusion externe :
  - C.N.A.M.(2)
  - C.R.A.M.(2)
  - C.G.S.S.(2)
  - Ministère des Affaires Sociales et de la Solidarité Nationale (DRT - DSS)
  - Directions Régionales du Travail et de la Main d'Oeuvre

- Diffusion interne :
  P / DG - DER - ETA - EG - INF - DN - FOR - SM
  N / DER - DS - DN - EP - Chrono

SIMULATION DE LA DYNAMIQUE DE L'ECOULEMENT ET DE LA DISPERSION D'UN POLLUANT A L'INTERIEUR D'UN LOCAL INDUSTRIEL VENTILE

1 - Méthodes numériques

J.R. FONTAINE, F. DELLAGI
Service Thermique, Ventilation, Eclairage, INRS, avenue de Bourgogne, B.P. 27, 54501 Vandoeuvre Cédex France

Résumé du projet de publication n° 1342

Dans cet article, une simulation numérique de deux configurations de ventilation est présentée. Cette simulation est basée sur la résolution des équations hydrodynamiques de la conservation couplées à un modèle de turbulence à deux équations.

L'étude de la dynamique de l'écoulement et le calcul du champ de vitesses en chaque point d'une enceinte ventilée a permis de mettre en évidence les zones de recirculation et les zones mortes. Comme application immédiate, la dispersion d'un polluant est étudiée. Ainsi, les régions de grande concentration ont été localisées et l'effet d'écran du jet d'eau sur la recirculation du polluant a été constaté.

Les résultats de la simulation numérique sont comparés avec ceux obtenus par simulation hydraulique. On note un bon accord dans l'ensemble.

ROOMVENT - 87

"AIR DISTRIBUTION IN VENTILATED SPACES"

International Conference

Stockholm 10-12 juin 1987

DYNAMICAL AND CONTAMINANT FLOW SIMULATION INSIDE VENTILATED INDUSTRIAL PREMISES I : NUMERICAL METHODS

J.R. FONTAINE, F. DELLAGI
Service Thermique, Ventilation, Eclairage, INRS, avenue de Bourgogne, BP 27, 54501 Vandoeuvre Cédex, France.

1 - Introduction

Our goal is to find reliable methods to be able to control the pollutants dispersion in industrial premises. The question is how to design the ventilation process of a factory containing pollutant sources in order to get concentrations (of dangerous materials) lower than the Threshold Limit Values.

In this paper we want to present an approach based on a computer simulation of the physical phenomenons entering into such processes. In particular, we shall consider two simple ventilation problems described as follows.

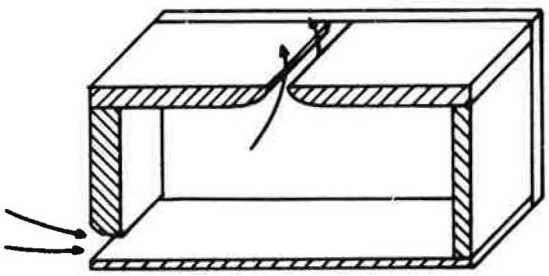

Fig. 1.1

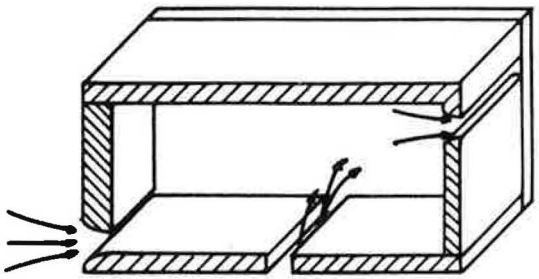

Sketch of the studied configurations

Fig. 1.2

Figure 1.1 schematises a room with an air inlet and an air outlet. The flow is supposed to be two-dimensional stationary and isothermal. The only adimensional number which characterizes the flow is the Reynolds number (Re). We consider a fully turbulent situation ($Re = 10^5$).

In figure 1.2, a polluting source has been added on the floor. The flow is defined by two numbers : Re and the Schmidt numbers. Again the flow is turbulent ($Re = 2.10^4$). As a matter of fact, because of turbulence, the molecular Schmidt number becomes irrelevant.

Both situations were also simulated in two hydraulic benches*. Case 1 (fig. 1.1) was designed to test experimentally the computation of the dynamics (the velocity field). In case 2, (fig. 1.2) the computation of the concentration field was tested [2].

The core of our computer program is largely inspired from the works of the Imperial College group [1].

The paper is organized as follows : section 2 contains a mathematical formulation of the problem and a brief description of the numerical methods.

Section 3 is devoted to the study of configuration 2 ; a comparison between numerical and experimental results is included. Section 4 contains the simulation of configuration 1. A first comparison with a few experimental results is also presented.

---

* For experimental purposes, it was easier to choose a different geometry in both cases.

2 - Description of the model

The physical assumptions are :
- two-dimensional flow,
- stationary flow,
- incompressible fluid,
- isothermal situation,
- passive pollutant.

The last assumption means that the introduction of pollutant in the cavity does not perturb the flow. This has been checked experimentally at least for small pollutant flows (pure water flow/pollutant flow ≃ 15) [2]. Given these hypotheses the phenomenon is described by the following equations :

$$\left|\begin{array}{l} \dfrac{\partial}{\partial x_i}(\rho u_i) = 0 \\ \dfrac{\partial}{\partial t}(\rho u_i) + \dfrac{\partial}{\partial x_j}(\rho u_i u_j) = -\dfrac{\partial p}{\partial x_i} + \dfrac{\partial}{\partial x_j}\left[\mu\left(\dfrac{\partial u_i}{\partial x_j} + \dfrac{\partial u_j}{\partial x_i}\right)\right] \\ \dfrac{\partial}{\partial t}(\rho c) + \dfrac{\partial}{\partial x_j}(\rho u_j c) = \dfrac{\partial}{\partial x_j}\left(\rho D \dfrac{\partial c}{\partial x_j}\right) \end{array}\right. \qquad (1)$$

The convention of summation on repeated indices bas been adopted :
u_i are the velocity components,
x_i and t are the space and time coordinates,
c denotes the pollutant concentration,
μ is the viscosity,
ρ is the density,
D is the pollutant diffusion coefficient.

Because of turbulence u_i, p, c are fluctuating functions of time. This implies that the numerical solution of these equations (at least for practical situations) would require a computational power which is well beyond what is now available on computers. We shall therefore adopt the traditional point of vue of solving the mean motion :

$$u_i = U_i + u'_i \quad ; \quad p = P + p' \quad ; \quad c = C + c'$$

U_i, P and C, are mean values (the mean being taken on a set of different realisations of the same configuration), and u'_i , p' and c' are fluctuating components.

Given the stationarity hypothesis, the equations for the mean motion reads :

$$\left|\begin{array}{l} \dfrac{\partial}{\partial x_i}(\rho U_i) = 0 \\ \dfrac{\partial}{\partial x_j}(\rho U_i U_j) = \dfrac{\partial}{\partial x_j}(-\rho \overline{u'_i u'_j}) - \dfrac{\partial P}{\partial x_i} + \dfrac{\partial}{\partial x_j}\left[\mu\left(\dfrac{\partial U_i}{\partial x_j} + \dfrac{\partial U_j}{\partial x_i}\right)\right] \\ \dfrac{\partial}{\partial x_j}(\rho U_j C) = \dfrac{\partial}{\partial x_j}(-\rho \overline{u'_j c'}) + \dfrac{\partial}{\partial x_j}\left(\rho D \dfrac{\partial C}{\partial x_j}\right) \end{array}\right. \qquad (2)$$

$\overline{}$ denotes the mean as defined above.

2.1 - Turbulence modeling

Equations (2) are similar to equations (1) up to two terms which have to be modeled. We are facing the usual closure problem.

We adopt the k - ε model of [3] described as follows :

- Gradient transport hypothesis (HINZE 1959) :

$$-\rho \overline{u_i' u_j'} = \mu_t \left(\frac{\partial U_i}{\partial x_j} + \frac{\partial U_j}{\partial x_i}\right) - k \delta_{ij}$$

$$-\rho \overline{u_j' c} = \frac{\mu_t}{S_t} \frac{\partial C}{\partial x_j}$$

μ_t is the turbulent viscosity, S_t is the turbulent Schmidt number, k is the turbulent kinetic energy.

- Dimensional analysis :

$$\mu_t = C_\mu \rho k^2/\varepsilon$$

where ε is the rate of dissipated turbulent energy and C_μ is an adimensional number to be specified later.

- k and ε obey the following transport equation [3] :

$$\frac{\partial k}{\partial t} + U_i \frac{\partial k}{\partial x_i} = \frac{\partial}{\partial x_i}\left(\frac{\mu_t}{\rho \sigma_k} \frac{\partial k}{\partial x_i}\right) + \frac{\mu_t}{\rho}\left(\frac{\partial U_i}{\partial x_j} + \frac{\partial U_j}{\partial x_i}\right) \frac{\partial U_i}{\partial x_j} - \varepsilon$$

$$\frac{\partial \varepsilon}{\partial t} + U_i \frac{\partial \varepsilon}{\partial x_i} = \frac{\partial}{\partial x_i}\left(\frac{\mu_t}{\rho \sigma_\varepsilon} \frac{\partial \varepsilon}{\partial x_i}\right) + C_{1\varepsilon} \frac{\varepsilon}{k} \frac{\mu_t}{\rho}\left(\frac{\partial U_i}{\partial x_j} + \frac{\partial U_j}{\partial x_i}\right) \frac{\partial U_i}{\partial x_j} - C_{2\varepsilon} \frac{\varepsilon^2}{k}$$

σ_k , C_μ, σ_ε, $C_{1\varepsilon}$, $C_{2\varepsilon}$ are empirical dimensionless constants which value (suggested by Launder and Spalding [3]) are :

σ_k	C_μ	σ_ε	$C_{1\varepsilon}$	$C_{2\varepsilon}$
1.0	0.09	1.3	1.44	1.92

Using the stationarity hypotheses the set of equations we have to solve is :

$$
\left|
\begin{aligned}
&\frac{\partial}{\partial x_i}(\rho U_i) = 0 \\
&\frac{\partial}{\partial x_j}(\rho U_i U_j) = -\frac{\partial P}{\partial x_i} + \frac{\partial}{\partial x_j}\left[\mu_{eff}\left(\frac{\partial U_i}{\partial x_j} + \frac{\partial U_j}{\partial x_i}\right)\right] \\
&\frac{\partial}{\partial x_j}(\rho U_j C) = \frac{\partial}{\partial x_i}\left(\frac{\mu_{eff}}{S_t}\frac{\partial C}{\partial x_i}\right) \\
&U_i \frac{\partial k}{\partial x_i} = \frac{\partial}{\partial x_i}\left(\frac{\mu_t}{\sigma_k \rho}\frac{\partial k}{\partial x_i}\right) + \frac{\mu_t}{\rho}\left(\frac{\partial U_j}{\partial x_i} + \frac{\partial U_i}{\partial x_j}\right)\frac{\partial U_i}{\partial x_j} - \varepsilon \\
&U_i \frac{\partial \varepsilon}{\partial x_i} = \frac{\partial}{\partial x_i}\left(\frac{\mu_t}{\rho\,\sigma_\varepsilon}\frac{\partial \varepsilon}{\partial x_i}\right) + C_{1\varepsilon}\frac{\varepsilon}{k}\frac{\mu_t}{\rho}\left(\frac{\partial U_i}{\partial x_j} + \frac{\partial U_j}{\partial x_i}\right)\frac{\partial U_i}{\partial x_j} - C_{2\varepsilon}\frac{\varepsilon^2}{k} \\
&\mu_t = \rho\, C_\mu \frac{k^2}{\varepsilon}
\end{aligned}
\right. \qquad (3)
$$

where $\mu_{eff} = \mu + \mu_t$.

From now on we use the notations : $U_1 = U$, $U_2 = V$, $x_1 = x$, $x_2 = y$.

The boundary conditions which characterize the particular flow we have to study will be specified later.
Equations (3) have to be discretized in order to be solved numerically.

2.2 - Discretization

2.2.1 - The Grid

Rectangular with arbitrary spacing.

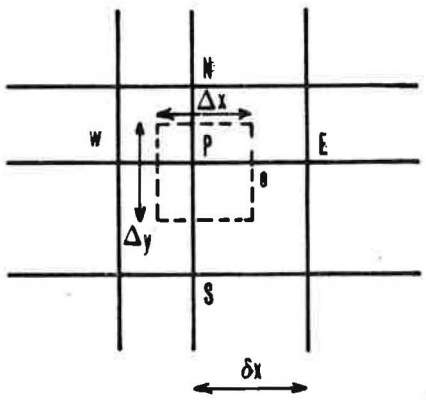

Fig. 3.1 : The grid

Scalar quantities P, C, k, ε are defined at the nodes of the grid. Vector quantities are defined in the middle of two nearest neighbour nodes (see fig. 3.2).

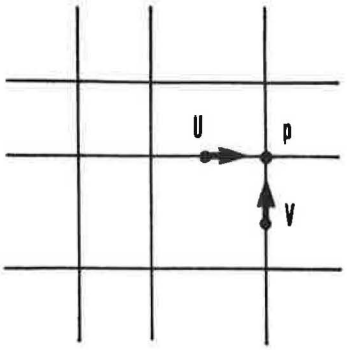

Fig. 3.2 : "Staggered" grid

Control volumes for scalars are defined by the dotted lines as in fig. 3.1.

2.2.2 - Discretized equations

All equations are of the form :

$$\vec{\nabla}.(\rho \vec{U} \phi - \Gamma_\phi \vec{\nabla} \phi) - S_\phi = 0 \qquad (4)$$

The discritized equation is obtained by integration of (4) in a control volume defined about each point P :

$$0 = \iint_V [\vec{\nabla}.(\rho \vec{U} \phi - \Gamma_\phi \vec{\nabla} \phi) - S_\phi] \, dV$$

$$= \int_{\partial V} (\rho \vec{U} \phi - \Gamma_\phi \vec{\nabla} \phi) \, d\vec{S} - \iint_V S_\phi \, dV$$

The surface integral is estimated by an hybrid scheme (see[4]).
The source term S_Φ is linearized :

$$S_\Phi = S_C + \Phi_P \, S_P$$

This leads to an equation :

$$a_P \Phi_P = a_E \Phi_E + a_W \Phi_W + a_S \Phi_S + a_N \Phi_N + b$$

where $a_E = \max (|0.5 * C_e|, D_e) - 0.5 * C_e$

$C_e = U_e \, \Delta y$

$D_e = (\Delta y / \delta X)$

a_N, a_S, a_N are defined similarly

$a_P = a_N + a_S + a_E + a_W - S_P$

Defining $P_e = \frac{C_e}{D_e}$, the scheme is central differences or upwind according to whether $|P_e| \leq 2$ or $|P_e| > 2$.

By discretization (3) is transformed into a set of algebraic equations. There is no equation for P. We use the SIMPLE algorithm to transform the continuity equation in an equation for P (see [4]). Whenever the boundary conditions are fixed, each equation is solved by the tridiagonal matrix algorithm [4].

2.2.3 - The boundary conditions

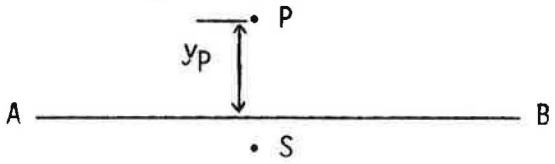

Fig. 4

If AB is a wall, the boundary conditions are :
U = 0, V = 0 on the wall,
k = 0, P = 0 for grid points just below the wall.
For grid points P just above the wall, the couplings between U_P and U_S or between k_P and k_S are replaced by a wall universal distribution function (this is done to avoid large gradients) : U_P is a linear or a logarithmic function of y_P according to whether p is in the laminar or turbulent sublayer. ε_P is obtained from k_P by a scaling argument [3] [1].

3 - The pollutant dispersion configuration

As mentioned in the introduction the laminar Schmidt number is irrelevant actually $D << \mu_t/S_t$. Even though we have no direct experimental information on S_t for the moment (this would require a simultaneous velocity concentration measurement) we choosed it to be 1, as it is usually done in the literature. We work with Re = 20.000, we do not think that there will be any difficulty to consider higher Re.

3.1 - Characterization of the flow

3.1.1 - Dynamical boundary conditions

These are explained in fig. 5.

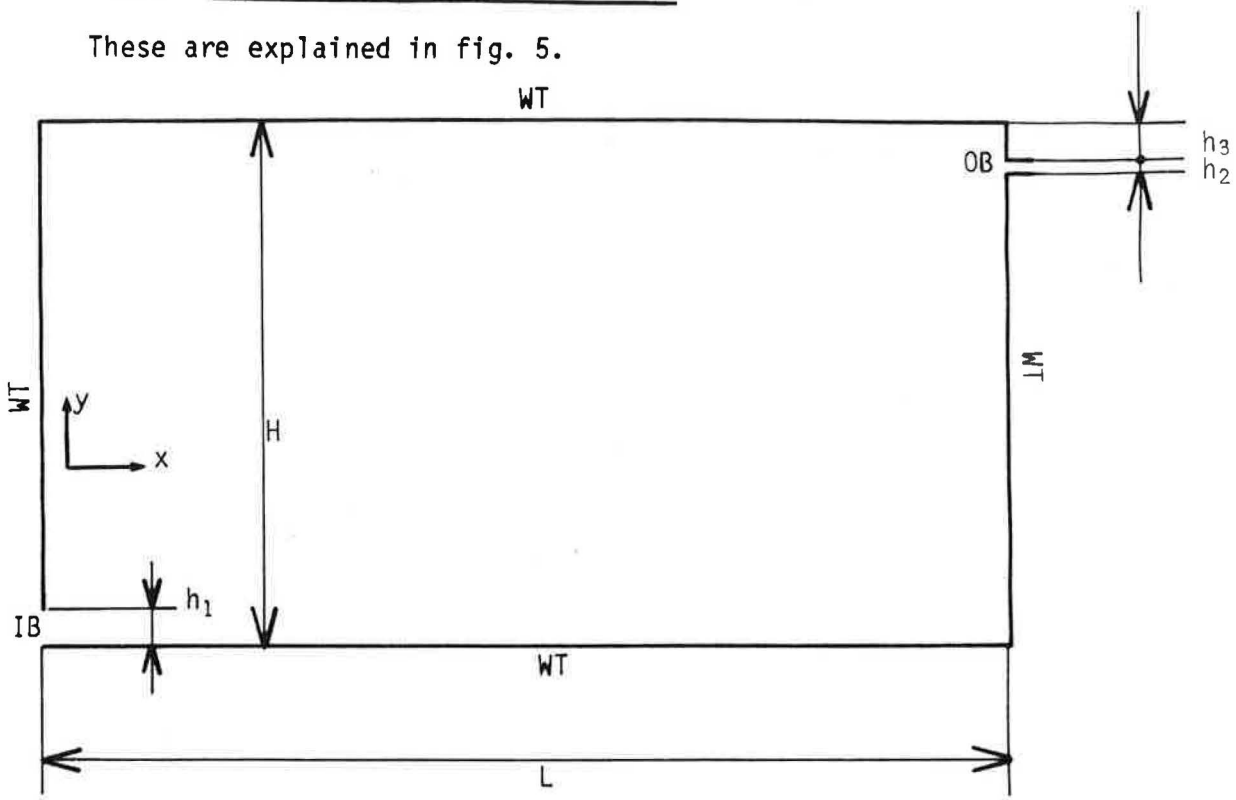

Fig. 5 : Description of the boundary condition

Geometry : H = . 7 ; L = 1.3 ; h_1 = . 025 ; h_2 = . 005 ; h_3 = . 05
UIN = 1

The units are such that :

$$Re_H = \frac{UIN * H}{\rho * \mu} = 20\ 000$$

Boundary conditions :

- WT means that a wall treatment has been applied (see 2.3.3). For instance for the east wall, we have : V = 0, P = 0, wall functions for U, k, ε.
- IB : inlet boundary conditions
  P = 0
  U = UIN = 1
  V = 0
  $k^2 = 0.06 * V^2$

  $$\varepsilon = \frac{k^{1.5}}{0.01 * H}$$

- OB : outlet boundary conditions
  $U = UIN * h_1 / h_2$
  V = 0
  P = 0

No boundary conditions for ε and k because at the outlet the scheme will be upwind.

3.1.2 - Pollutant boundary conditions

- No pollutant flux through each wall ($\partial_n C = 0$) except through the outlet.
- Modelisation of pollutant emission in the south wall.
  For easiness we assumed that the pollutant emission had no influence on the dynamics of the flow. The pollutant generation is therefore simulated by the source terms in the equation for C :

$$a_P C_P = a_N C_N + a_S C_S + a_E C_E + a_W C_W + S_C$$

$$S_C = a\, C_P + b_P$$

For all points P located in the rectangle R (see fig. 6), we took a = 0 and b_p = constant. We imposed no flux through AB to avoid a migration of pollutant through the south wall. b_p was choosen such that :

$$\sum_{p \in R} b_p = UIN * h_1 * \rho$$

Since the concentration equation is linear and second order and since we have only conditions on fluxes, we must impose a condition on C at some point in the cavity, to have a well defined solution. Because of our simple modelisation, it appears convenient to use a measured ouantity of C for a point P_o located in the pure water jet (the coordinates of P_o are : x = . 36 L, y = h_1/2).

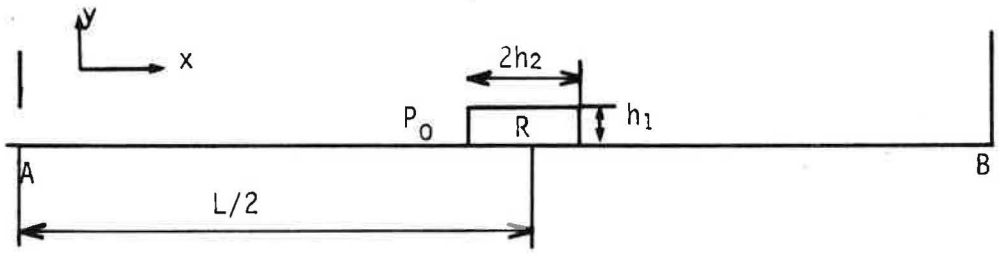

Fig. 6

3.2 - Numerical simulation and results

Because of the rather difficult boundary conditions (h_2/H = 140) we had to use a very fine grid : 54 x 47 nodes (see fig. 7). It appears that along the walls our first row of points was in the laminar sublayer. About 700 iterations were necessary to get a bona fide converging solution. All equations were verified with a global maximal error of a few percents (≃ 3 %). The computation took about 5 minutes of CPU time on a IBM 3090 computer.

3.2.1 - Results

The velocity field is displayed on fig. 8. A large recirculating zone is manifest. The jet flows along the boundaries.

A few isoconcentration curves are shown in fig. 9. The pollutant is redistributed everywhere in the cavity by convection and turbulent diffusion. The incoming jet of pure water has a screening effect on the recirculation of pollutant as can be seen from curves (1) and (2). Highest concentrations are located in the south right corner of the cavity (which corresponds to a small corner vortex as can be seen from the velocity map) and of course in the pollutant jet.

3.2.2 - Comparison with experiment

Experimental and computed results are compared through vertical concentration profiles (see fig. 10.1 - 10.8). For most points the agreement is better than 20 %. The highest discrepancy arises in the vicinity of the pollutant source where our modelisation is too naïve and where the experimental uncertainties are also high.

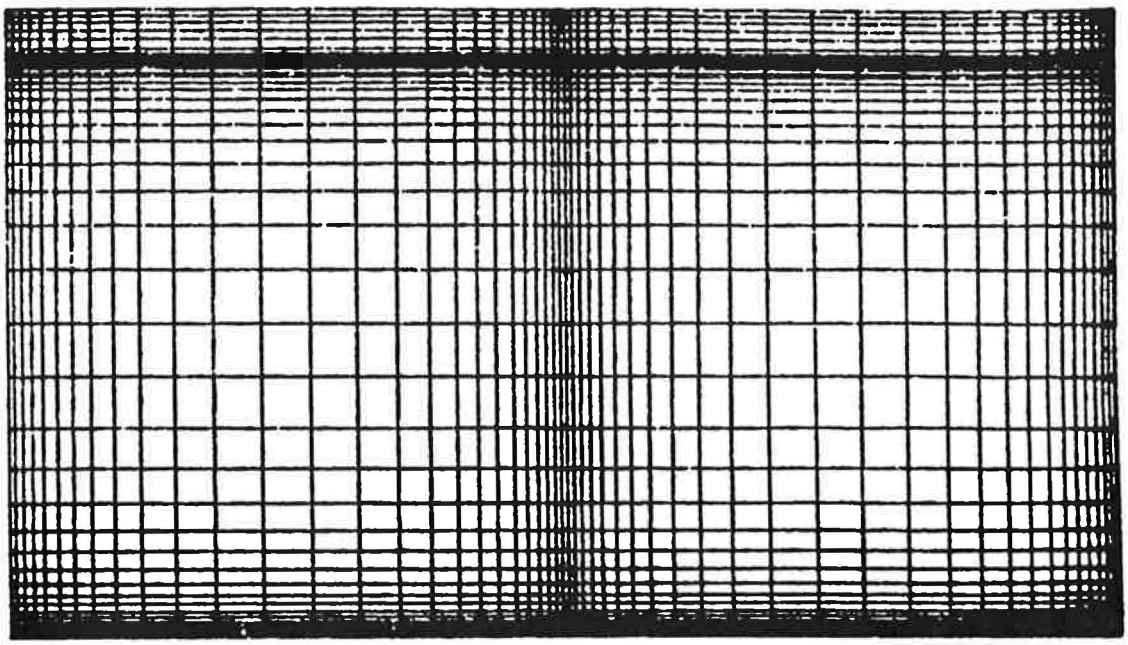

Fig. 7 : GRID 54 x 47 (used for the computation associated to the configuration of fig. 1.2)

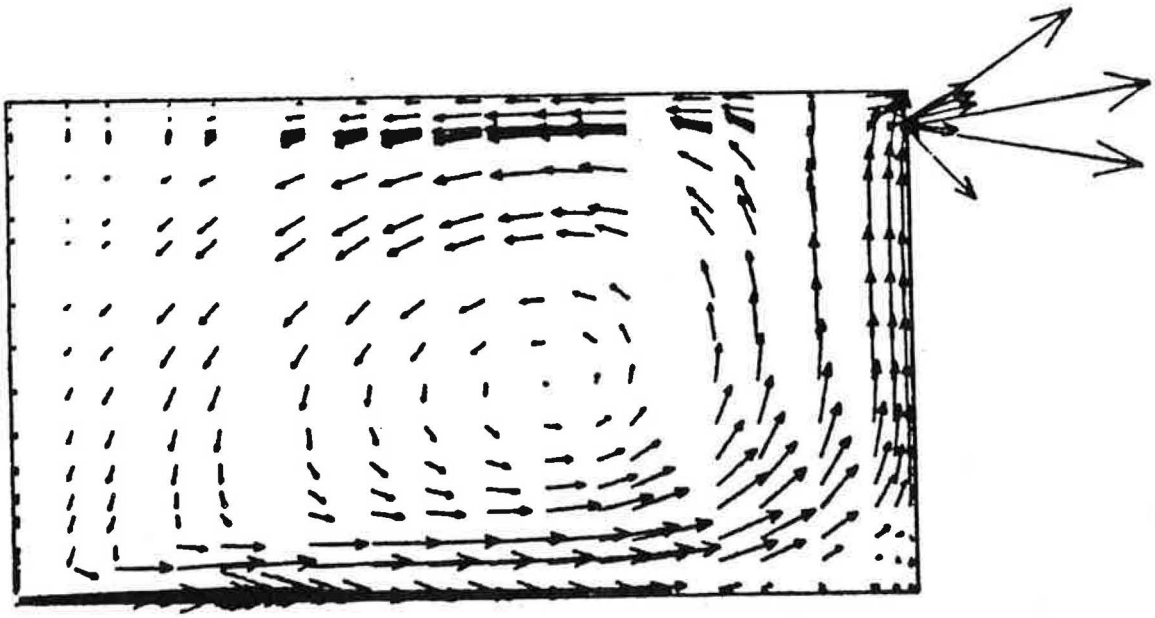

Fig. 8 : VELOCITY FIELD (configuration of fig. 1.2 : see 3.1)
Re_H = 20.000

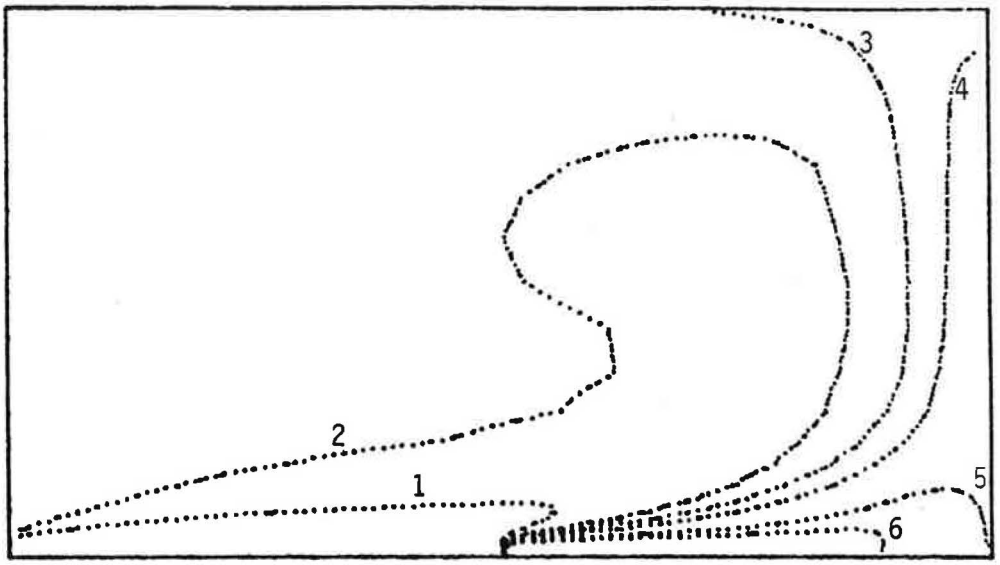

Fig. 9 : ISOCOCENTRATION CURVES (normalized by the exhaust concentration)

1 C = .62
2 C = .87
3 C = .99
4 C =1.19
5 C =1.61
6 C =1.85

Vertical concentration profiles

Concentrations $\tilde{c}$ are normalized by the exhaust concentration. Lengths ($\tilde{x}$, $\tilde{y}$) are normalized by the height H of the cavity.

Fig. 10.1
$\tilde{x}$ = .036

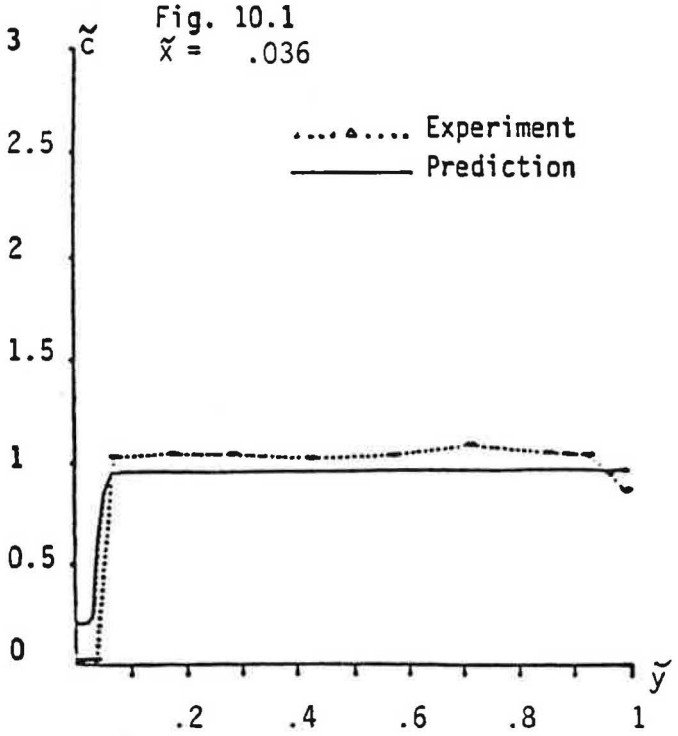

Fig. 10.2
$\tilde{x}$ = .36

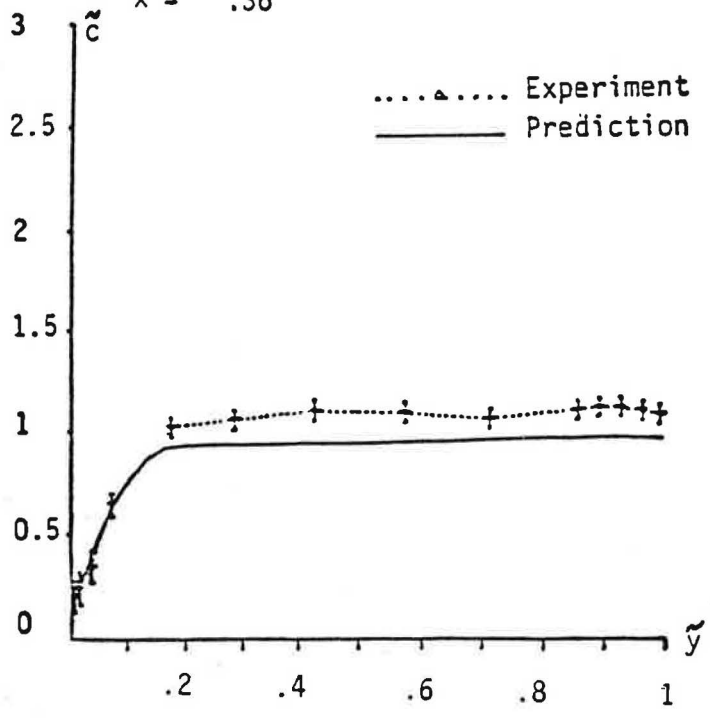

Vertical concentration profiles

Concentrations $\tilde{c}$ are normalized by the exhaust concentration. Lengths ($\tilde{x}$, $\tilde{y}$) are normalized by the height H of the cavity.

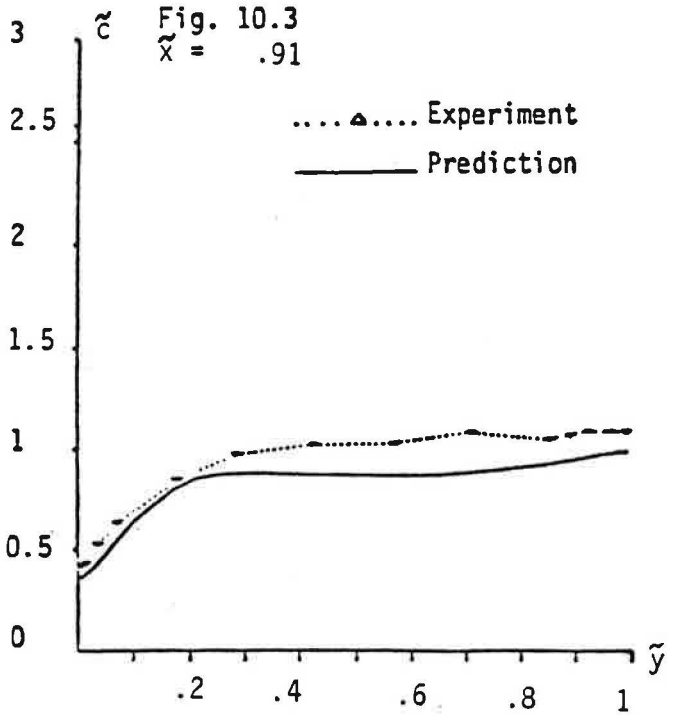

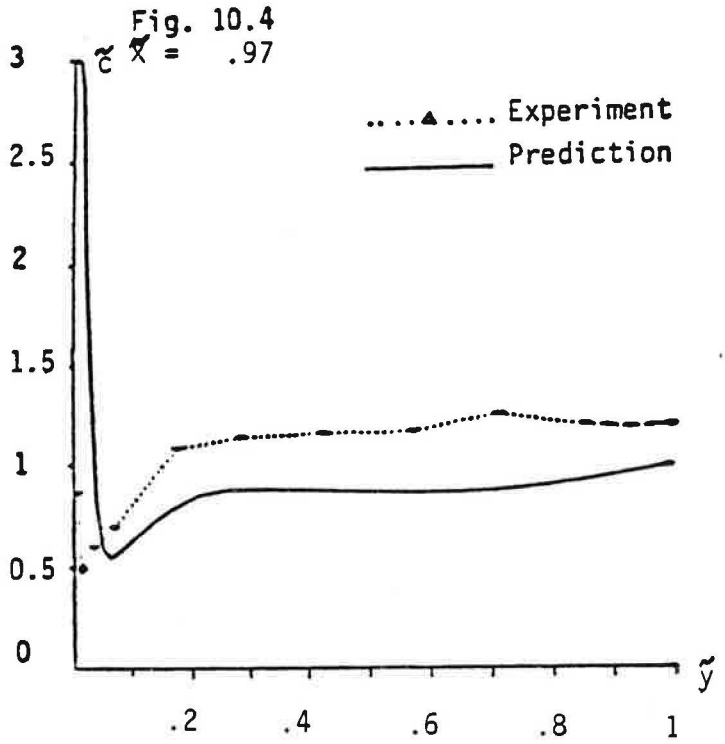

Vertical concentration profiles

Concentrations $\tilde{c}$ are normalized by the exhaust concentration. Lengths ($\tilde{x}$, $\tilde{y}$) are normalized by the height H of the cavity.

Fig. 10.5
$\tilde{x}$ = 1.14

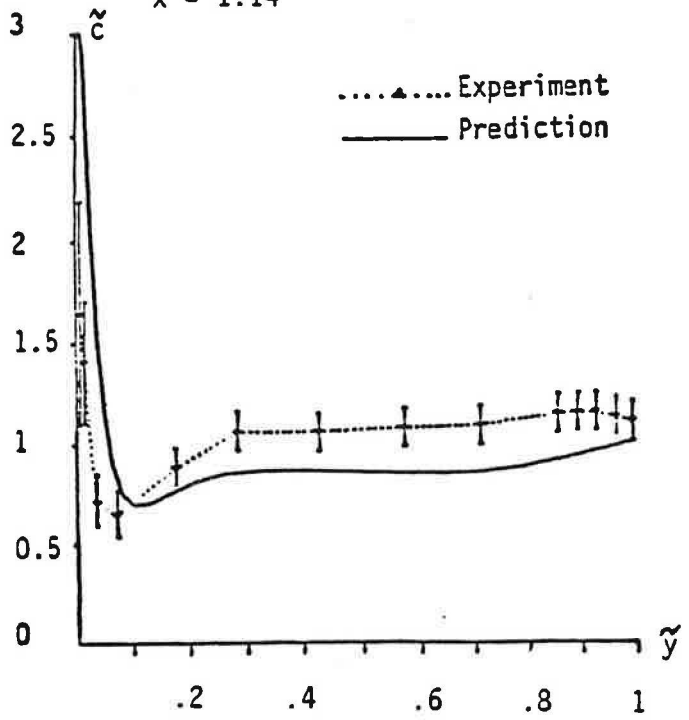

Fig. 10.6
$\tilde{x}$ = 1.32

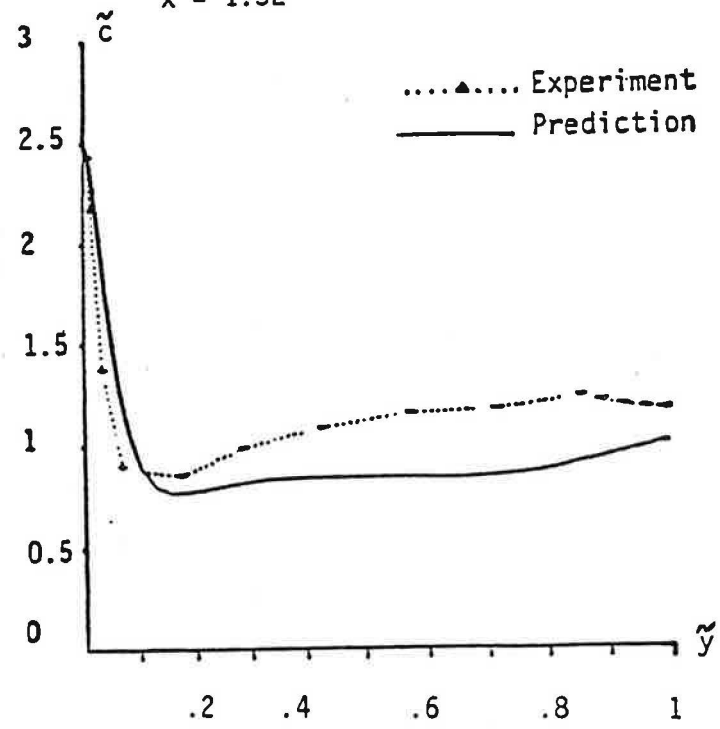

Vertical concentration profiles

Concentrations $\tilde{c}$ are normalized by the exhaust concentration. Lengths ($\tilde{x}$, $\tilde{y}$) are normalized by the height H of the cavity.

Fig. 10.7
$\tilde{x}$ = 1.57

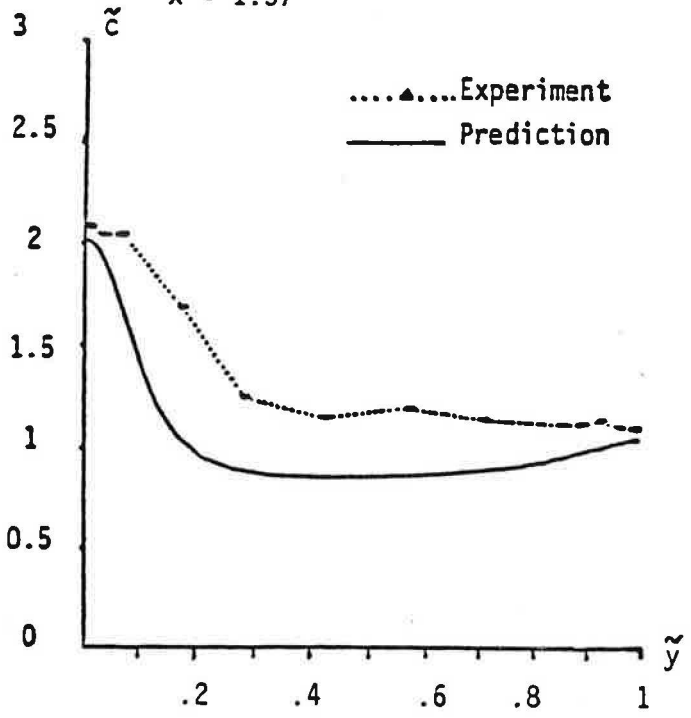

Fig. 10.8
$\tilde{x}$ = 1.83

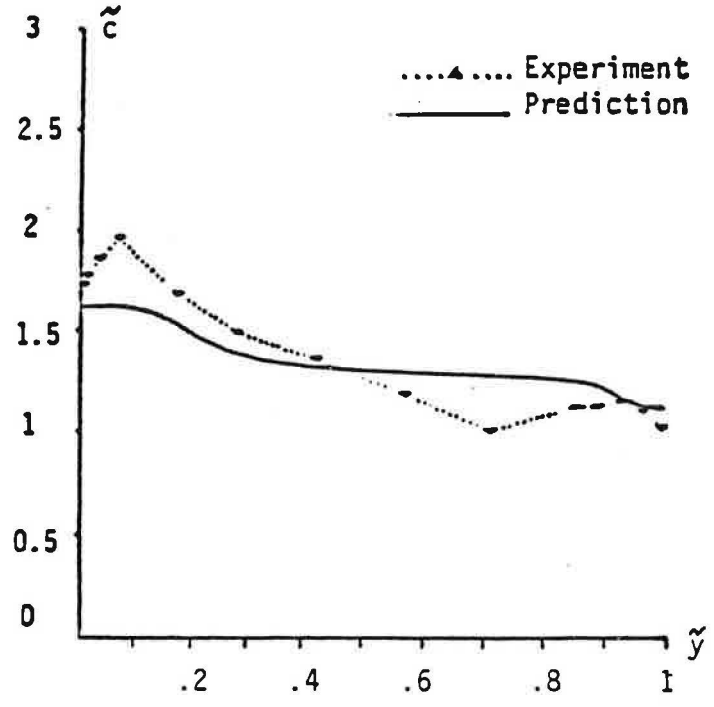

4 - The dynamical problem

In this section, we consider the dynamical problem, associated to the ventilation configuration (1). The geometry of the cavity is described in fig. 11.

The numerical simulation was carried out for a Reynolds number of 100 000 under steady and isothermal conditions.

4.1 - Boundary conditions

As priviously, wall treatments were adopted for the boundary layers (see fig. 11).

In the inlet, a constant velocity profil was applied (U = UIN = 1).

Boundary conditions :

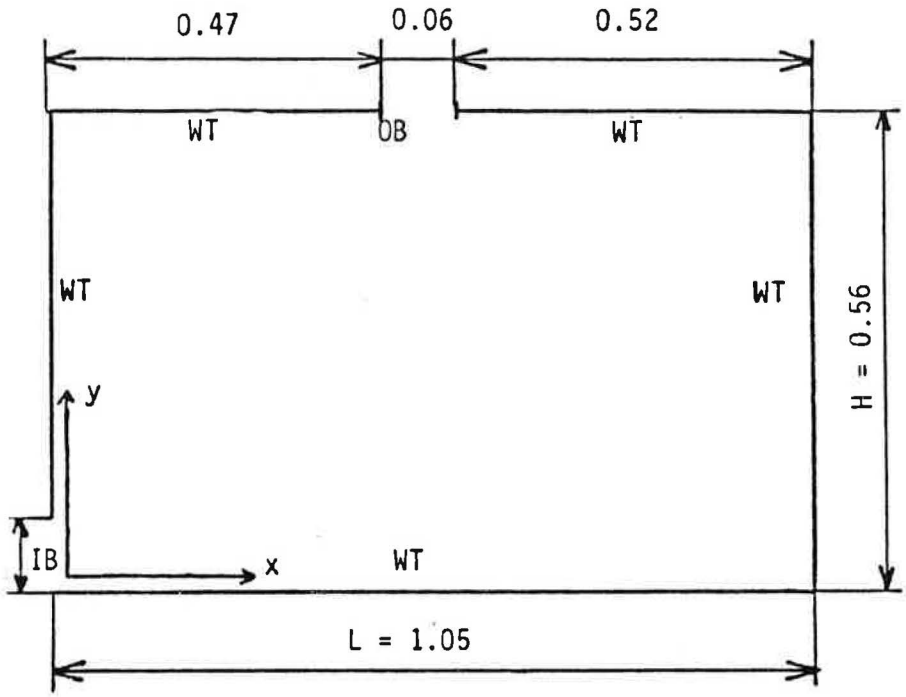

Fig. 11 : Description of the boundary conditions

(The units are such that $Re_H = \frac{UIN * H}{\rho * U} = 100.000$).

WT : means a wall treatment was applied

IB (Inlet) : $U = UIN = 1$
$V = 0$
$P = 0$
$k^2 = 0.03\ U^2$
$\varepsilon = K^{1.5}/0.005*h$

OB (Outlet) : $U = 0$
$V = UIN = 1$
$k^2 = 0.03\ U^2$
$\varepsilon = K^{1.5}/0.005*h$

4.2 - The grid

The grid was choosen in order to take into account large gradient regions, where the mesh was refined (near the walls and in the openings). Larger mesh was adopted elsewhere in the cavity, where small variable variations are expected. The grid was composed of 42 x 30 cells that progress exponentially in size as following :

$$\Delta X_i = EPSX * \Delta X_{i-1} \qquad \text{with } EPSX = 1.1$$

4.3 - Numerical results

Convergence was obtained after 400 iterations. The computation time was 1 mn. 37 CPU on IBM 3090.

4.3.1 - The velocity field and profiles

The flow configuration obtained for the mean motion is shown in fig. 12 A large recirculating eddy appears in the cavity. The center of this vortex is located in the center of the cavity. The jet reaches the east wall. We can notice the low velocities in the middle of the cavity. A very small vortex can be seen in the lower right corner below the jet. Figures 13 represent the evolution of the U componant vertical profile starting at the inlet (x = 0.05).

4.3.2 - Velocities fluctuations profiles

Figure 14.a represents vertical velocity fluctuations profile of $(k/V\overline{U^2} + \overline{V^2})$ at the inlet (x = 0.05). Small fluctuations can be observed in the jet region. A jump appears at the boundary between the jet and the large vortex. High fluctuations are also observed in the vicinity of the upper left corner.

Figure 14.b represents the vertical velocity fluctuations profile in the middle of the cavity (x = 0.5). Here the fluctuations present a maximum in the middle of the cavity (where velocities are low). They are relatively small elsewhere.

4.4 - Comparative experiment

An experiment was run out in a water bench test (see [2]). The same conditions were satisfied such as :
- isothermal flow,
- proportional geometrical dimensions,
- Reynolds number Re_H= 100 000.

4.4.1 - Qualitative comparison of computated and measured velocities maps

The predictions are in agreement with the finding of the experiments in the following respects :
- one large recirculating eddy appears in the cavity,
- the jet reaches the east wall.

4.4.2 - Quantitative analysis of numerical and experimental results

Figure 15 displays comparison between a calculated and a measured vertical U velocity profile : (X/L = 0.86).

Both results agree within 20 % in the lower part. Higher discrepancy appears in the upper part. In particular the experimental datas show absence of flux conservation. This is presumably produced by a weak mean velcocity component perpendicular to the measuring plane. This fact is under experimental unvestigations (see [2]).

4.5 - Conclusion

The predicted velocity field was in good agreement in the lower part of the cavity. Work in progress seeks to obtain better agreement specially in the upper part of the cavity. The twodimensional character of the flow will be checked experimentally. On the other hand, improvements in the k - ε model and boundary conditions, specially the velocity profile in the inlet will be done.

REFERENCES

[1] GOSMAN, F.J.K. IDERIAH
A general computer program for two dimensional turbulent recirculating flow.
Department of mechanical Engineering.
Imperial College - LONDON (1976).

[2] GARDIN P., BERLANDIER P., SERIEYS J.C.
Dynamical and contaminant flow simulation inside ventiladed industrial premises 2 : experimental methods.
I.N.R.S. (1987). (Submitted to this conference).

[3] LAUNDER B.E., SPALDING D.B.
"The numerical computation of turbulent flows" - Comp. Methods in Applied Mechanics and Engineering, 3 pp 269, 289 (1974).

[4] PATANKAR, S.V.
Numerical heat transfer and fluid flow in computational methods in mechanics and thermal sciences.
MINKOWYCZ and SPARROW editors. Hemisphere publishing corporation - WASHINGTON - NEW-YORK - LONDON (1980).

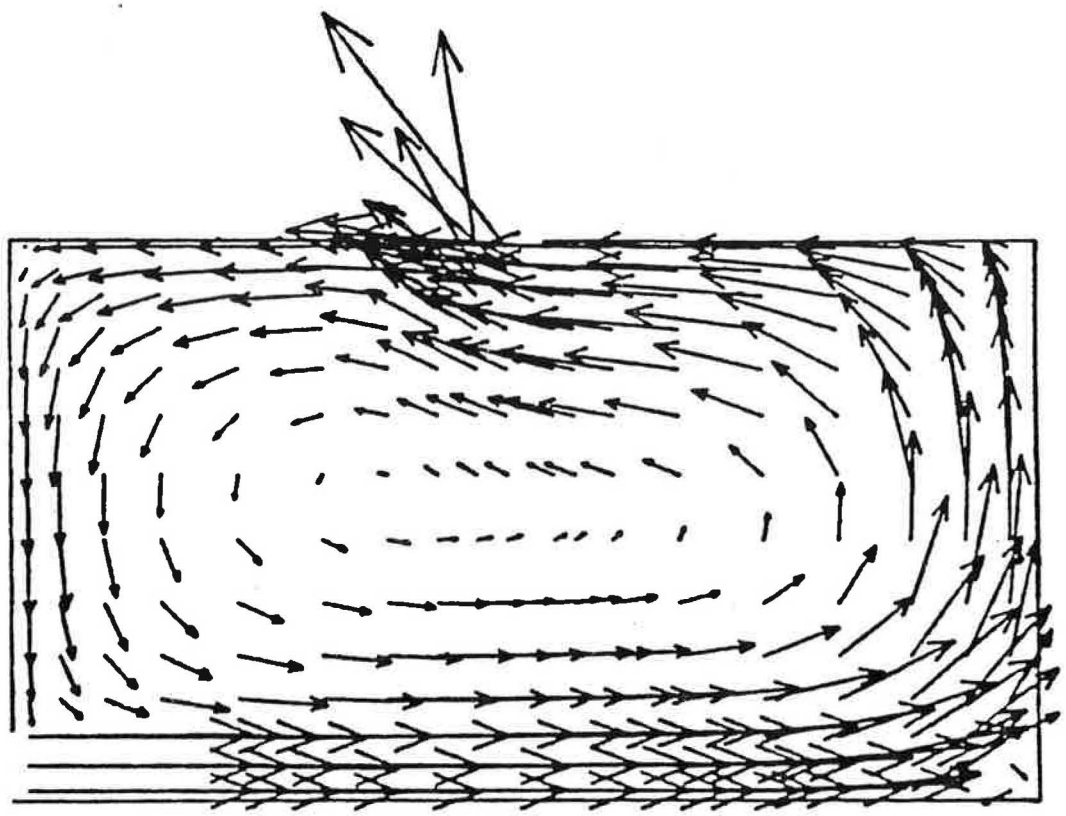

Fig 12a : Computed velocity field in the cavity (Re_H=100.000)
Cavity described on figure 11

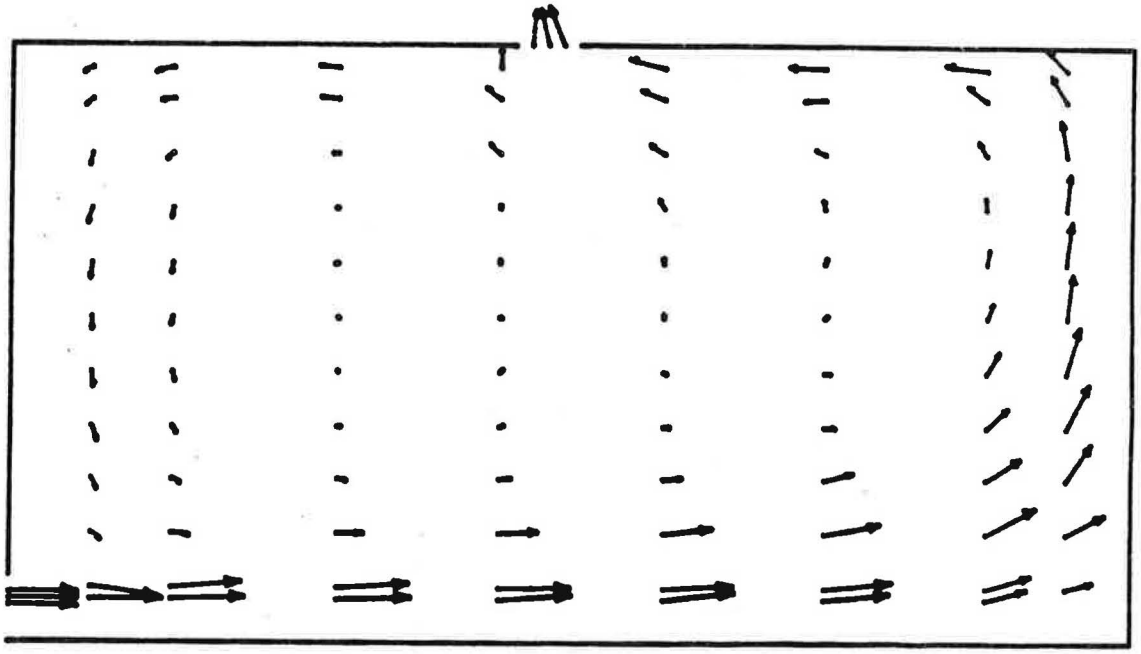

Fig 12b : Measured velocity field in the cavity

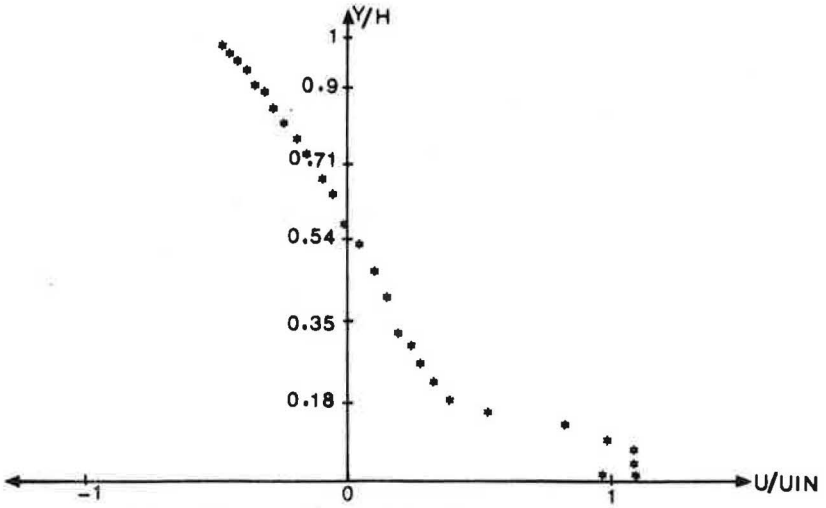

Fig 13.a : U vertical profile at x = 0.45 H

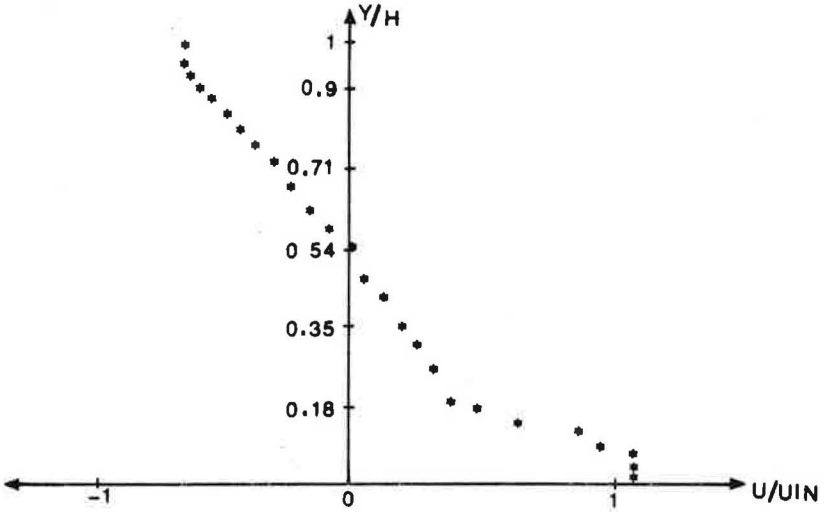

Fig 13.b :U vertical profile at x = 0.9 H

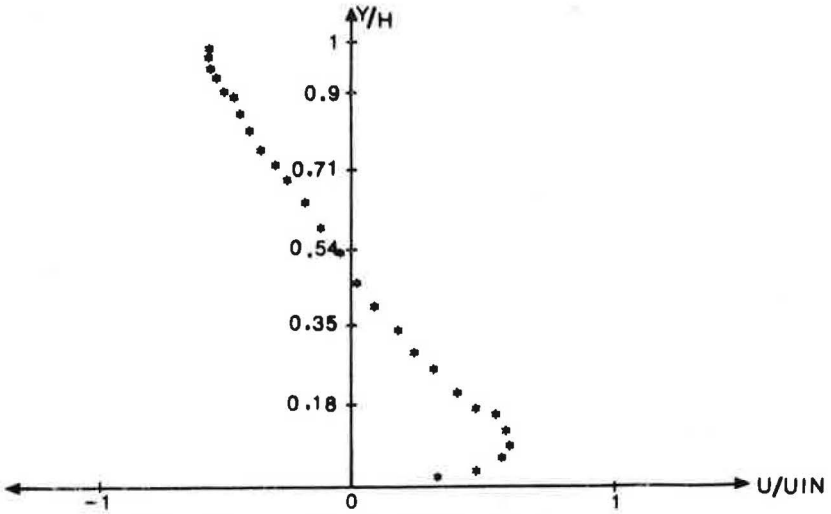

Fig 13.c : U vertical profile at x = 1.6 H

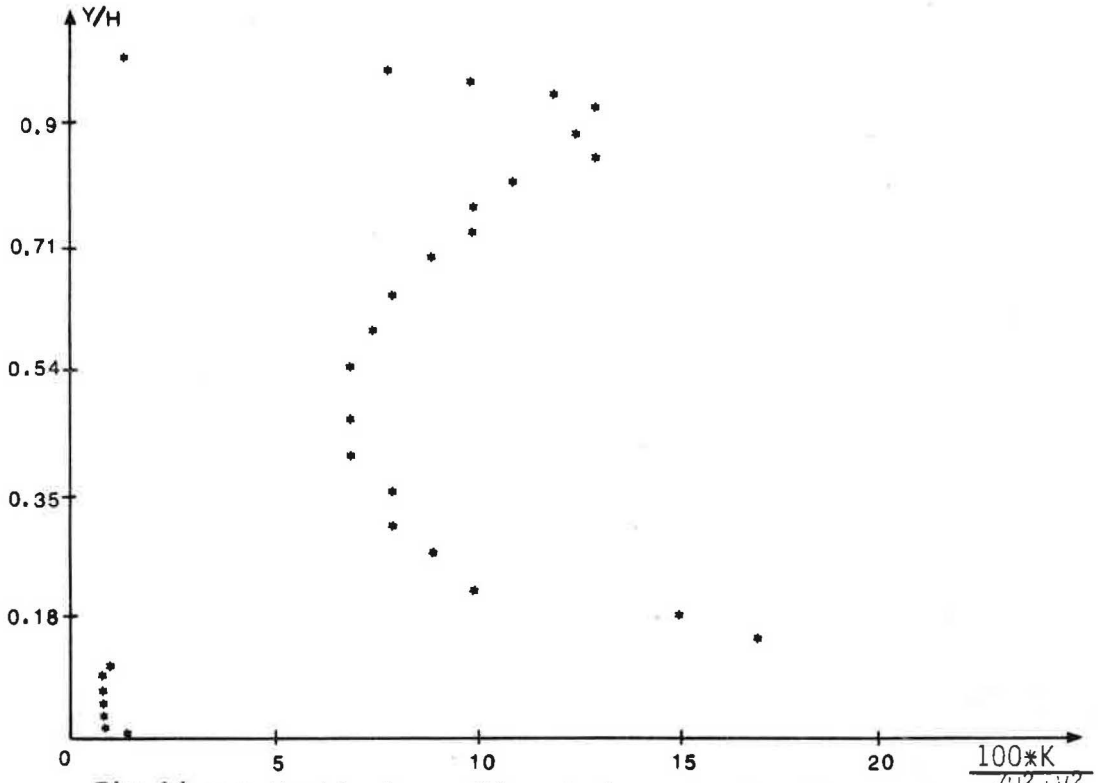

Fig 14.a : Vertical profile of the velocity fluctuations at x = 0.09H

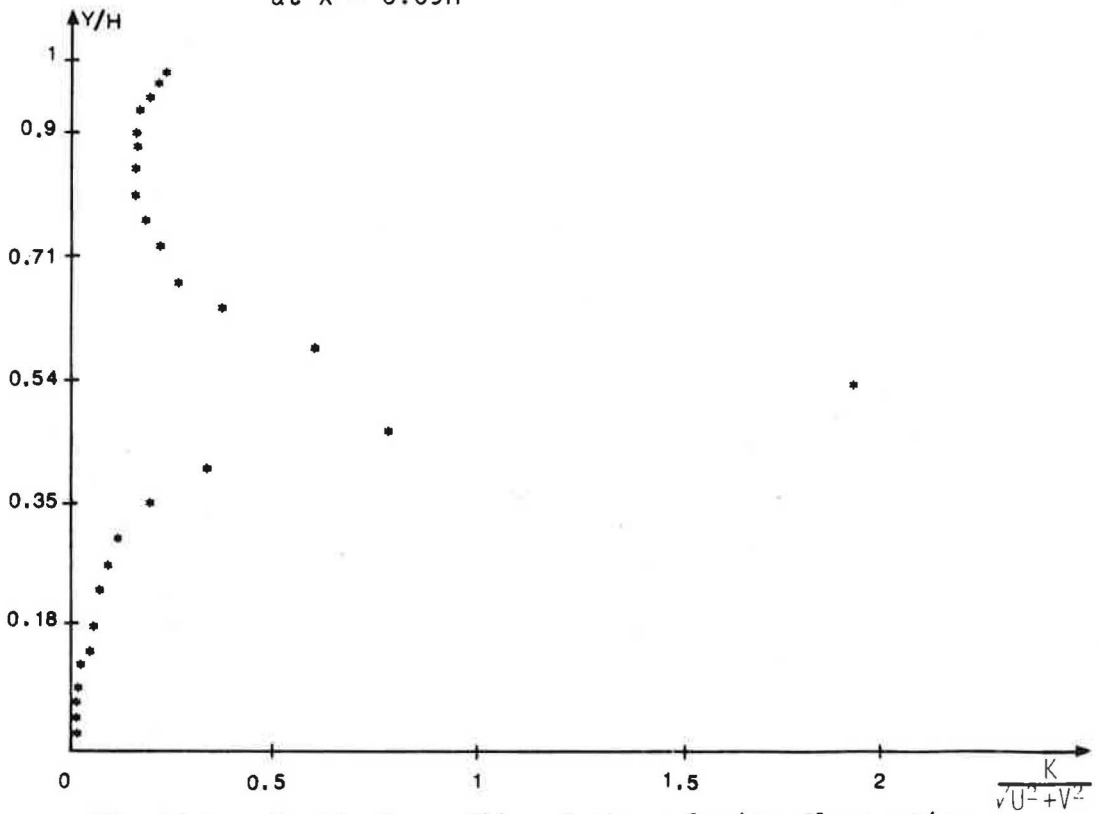

Fig 14.b : Vertical profile of the velocity fluctuations at x = 0.9H

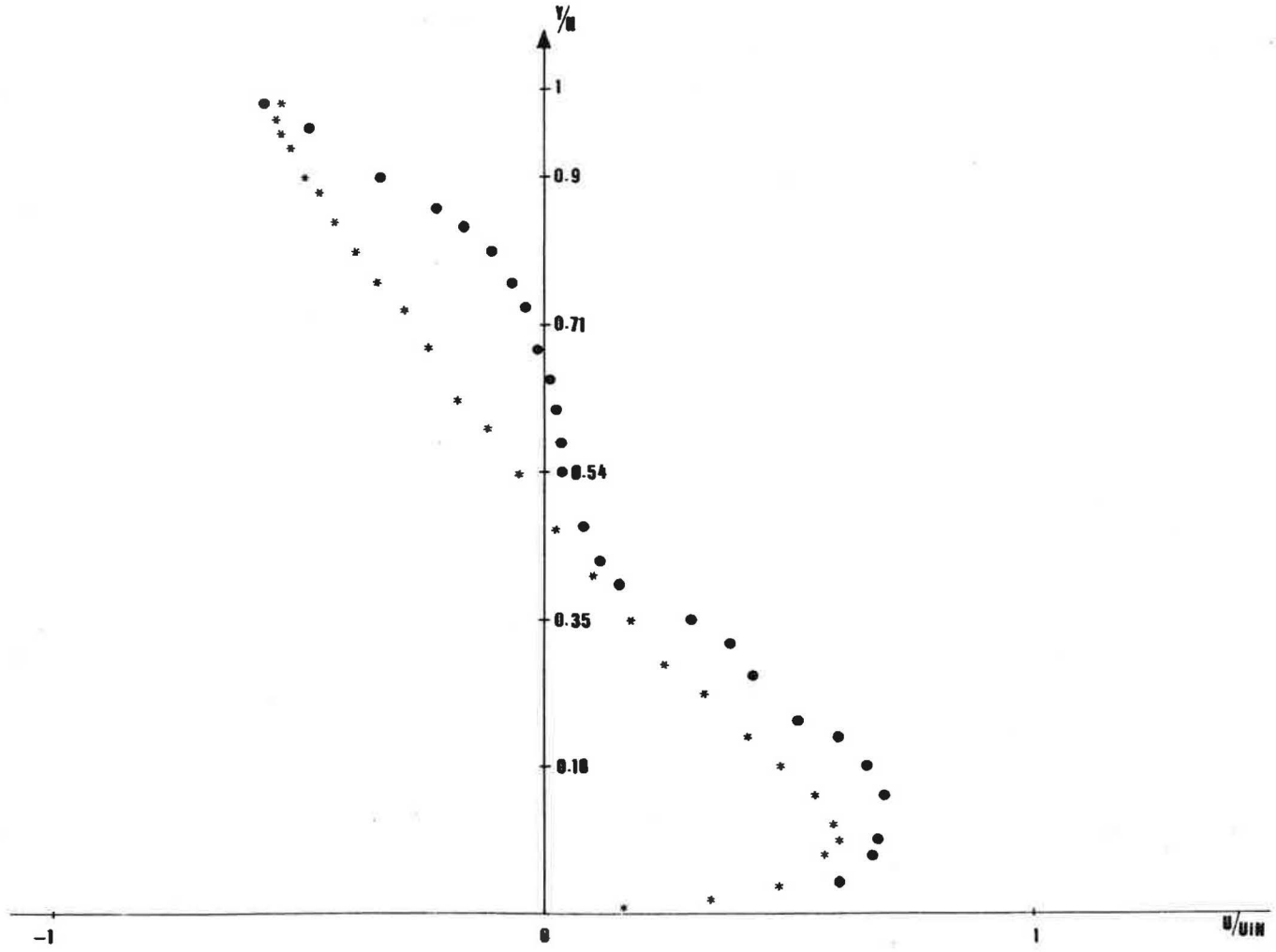

U vertical profile at x = 1.6 H - Comparison between numerical (*) and experimental (•) results